

Interplay between disorder, local relaxation, and collective behavior for an ensemble of emitters outside versus inside a cavity

Zeyu Zhou *Department of Chemistry, University of Pennsylvania, 231 South 34th Street, Philadelphia, Pennsylvania 19104, USA*

Hsing-Ta Chen

Department of Chemistry, University of Pennsylvania, 231 South 34th Street, Philadelphia, Pennsylvania 19104, USA and Department of Chemistry and Biochemistry, University of Notre Dame, 251 Nieuwland Science Hall, Notre Dame, Indiana 46556, USA

Joseph E. Subotnik

Department of Chemistry, University of Pennsylvania, 231 South 34th Street, Philadelphia, Pennsylvania 19104, USA

Abraham Nitzan

Department of Chemistry, University of Pennsylvania, 231 South 34th Street, Philadelphia, Pennsylvania 19104, USA and Department of Chemistry, Tel Aviv University, Tel Aviv 69978, Israel

(Received 5 December 2022; revised 27 March 2023; accepted 27 June 2023; published 9 August 2023)

The interplay between collective optical response and molecular static and dynamic disorder is studied using simple effective Hamiltonians for an ensemble of two-level emitters inside and outside a single-mode cavity. We model environmental disorder by randomly modulating the molecular transition frequencies and the coupling between the emitters and the electromagnetic field. We also consider the effects of intermolecular interactions and orientational disorder. We investigate how these effects lead to new features in the steady-state absorption (outside the cavity), transmission spectra (inside the cavity), and the yield of local molecular processes such as a unimolecular reaction. Outside the cavity, the collective behavior is manifested in the linewidth of the steady-state absorption, the emission spectrum, and the local chemical yield. Inside the cavity, however, the collective behavior primarily determines the Rabi splitting. The effects of intermolecular interactions under orientational disorder are also studied. For the most part, for all types of disorder, if we increase disorder, we find a reduction in the collective nature of the molecular response (smaller effective N) and therefore the Rabi splitting contraction occurs with orientational disorder. Moreover, we find that static disorder is more destructive to collective behavior than dynamic disorder.

DOI: [10.1103/PhysRevA.108.023708](https://doi.org/10.1103/PhysRevA.108.023708)

I. INTRODUCTION

Understanding the interplay between collective molecular optical response and molecular disorder has drawn a great deal of interest in recent years. Collective optical response can be seen in the time domain—for instance, Dicke superradiance emission [1–5], superfluorescence [6,7], and superabsorption [8] have been discussed extensively in the literature—or in the frequency domain, e.g., in optical cavities where collective response is manifested in the observed Rabi splitting that characterizes the strong light-matter coupling regime in such a system. Near a metal interface and in optical cavities, the response of an individual molecule is affected also by the confined character of the cavity as demonstrated by the Purcell effect as well as different realizations of surface-enhanced spectroscopies [9–28]. The collective response is characterized by a nontrivial dependence of experimental observables on the number N of involved molecules; for example, one finds a rate linear in N for superradiance emission and a Rabi splitting \sqrt{N} in the optical response of molecular optical cavities. The dependence of these behaviors on

local disorder has been the subject of several recent studies [29–54].

In this paper we discuss the effect of different types of disorder on the collective optical response of molecular systems in and out of the cavity using two simple models: site energy disorder and coupling disorder. We also discuss how the interplay between the collective optical response (outside vs inside a single-mode cavity) and local molecular processes might affect the yield of molecular photoprocesses such as photochemical reactions.

II. MODEL AND CALCULATION METHOD

A. Molecular ensemble in the single-exciton subspace

Consider an ensemble of molecules with two electronic (ground and excited) states whose spatial extent is assumed shorter than the wavelength of its resonant absorption, subjected to pumping by a nearly resonant classical field. In addition, each molecular excited state can decay due to interaction with its local environment or a local chemical process.

The time evolution of this system can be described by the following Hamiltonian [30,31,34,55]:

$$\hat{H} = \hat{H}_0 + \hat{V}_{\text{pump}} - i\Gamma_{\text{rad}}\hat{Q} - i\Gamma_{\text{loc}}\hat{C}, \quad (1)$$

$$\hat{H}_0 = E_0|0\rangle\langle 0| + \sum_m E_m|m\rangle\langle m|, \quad (2)$$

$$\hat{V}_{\text{pump}} = \sum_m V_{0m} \cos(\omega t)|0\rangle\langle m| + V_{m0} \cos(\omega t)|m\rangle\langle 0|, \quad (3)$$

$$\hat{Q} = \sum_{m,m'} |m\rangle\langle m'|, \quad (4)$$

$$\hat{C} = \sum_m |m\rangle\langle m|. \quad (5)$$

In Eqs. (1)–(5), the molecular states are $\{|0\rangle, |m\rangle\}$: $|0\rangle = \prod_j |g_j\rangle$ is the total ground state and $|m\rangle = |x_m\rangle \prod_{j \neq m} |g_j\rangle$ is a singly excited molecular state. Note that we are working in a single-exciton basis, so our model can describe only weak excitations where many-exciton correlations can be disregarded [31,34,56–58]. The radiative emission of the molecules is treated implicitly using the effective non-Hermitian operator $-i\Gamma_{\text{rad}}\hat{Q}$ that arises when one considers one idealized wideband radiative continuum (with density of state ρ_{DOS}) coupled identically to all molecular emitters ($V_j = V_{\text{rad}} \forall j$), leading to the purely imaginary self-energy

$$\Gamma_{\text{rad}} = 2\pi \rho_{\text{DOS}} |V_{\text{rad}}|^2. \quad (6)$$

If we denote the wave function of the molecular system by $c_m(t)$, then under radiative pumping of the molecules, the outgoing radiative flux at any given time t is

$$J_{\text{rad}}(t) = \sum_{m,m'} \Gamma_{\text{rad}} c_m(t) c_{m'}^*(t). \quad (7)$$

Finally, $-i\Gamma_{\text{loc}}\hat{C}$ represents decay through a local channel involving a single-molecule process. In contrast to the radiative decay, this channel describes a process defined by the state of each individual molecule (and does *not* depend on intermolecular coherence). The outgoing local flux at any given time t is

$$J_{\text{loc}}(t) = \sum_m \Gamma_{\text{loc}} |c_m(t)|^2. \quad (8)$$

Note that in the Hamiltonian (1), pumping is done by a continuous-wave (cw) field at the driving frequency ω . Therefore, if we plot total steady-state outgoing flux $J_{\text{rad}} + J_{\text{loc}}$ as a function of this frequency ω , we obtain the steady-state absorption spectrum.

B. Molecular ensemble in an optical cavity

To describe the same molecular ensemble (also in the long-wavelength approximation) inside a single-mode optical cavity [59] (which assumes only the mode close to the relevant molecular transition is considered) under the condition that the molecular ensemble reaches the electronic strong-coupling regime, we modify the Hamiltonian (1)–(5) in several ways [60]. First, the external pumping does not directly couple to the emitters, but instead to the cavity mode $|v\rangle$. Second, the molecules do not couple directly to the far electromagnetic (em) field and are assumed to couple only to the cavity mode. Hence, the term $-i\Gamma_{\text{rad}}\hat{Q}$ is replaced by the

coupling term [Eq. (11) below]. Finally, the radiative ($\Gamma_{\text{cav}}^{(R)}$) and nonradiative ($\Gamma_{\text{cav}}^{(NR)}$) decay rates of the cavity mode to the far field and to damping in the cavity mirrors, respectively, are taken into account. The corresponding Hamiltonian is

$$\hat{H} = \hat{H}_0 + \hat{V}_{\text{cav-mol}} + \hat{V}_{\text{pump}} - i\Gamma_{\text{loc}}\hat{C} - i\Gamma_{\text{cav}}|v\rangle\langle v|, \quad (9)$$

$$\hat{H}_0 = E_v|v\rangle\langle v| + E_0|0\rangle\langle 0| + \sum_m E_m|m\rangle\langle m|, \quad (10)$$

$$\hat{V}_{\text{cav-mol}} = \sum_m V_{vm}|v\rangle\langle m| + V_{mv}|m\rangle\langle v|, \quad (11)$$

$$\hat{V}_{\text{pump}} = V_{0v} \cos(\omega t)|0\rangle\langle v| + V_{v0} \cos(\omega t)|v\rangle\langle 0|, \quad (12)$$

$$\hat{Q} = \sum_{m,m'} |m\rangle\langle m'|, \quad (13)$$

where v is the excited state of the cavity mode (and the ground state $|0\rangle$ refers to both the cavity and the molecular systems). Similar to many previous works, we consider only a single cavity mode and in correspondence to the single-exciton model, we include only the ground and first excited states of this mode.

Here the cavity photon leaking rate ($\Gamma_{\text{cav}} = \Gamma_{\text{cav}}^{(R)} + \Gamma_{\text{cav}}^{(NR)}$) determines the quality factor $\hbar\omega_{\text{cav}}/\Gamma_{\text{cav}}$. In addition to the local relaxation channel [which is the same as in Eq. (8)], the outgoing radiative flux through the cavity is

$$J_{\text{cav}}(t) = \Gamma_{\text{cav}}^{(R)} |c_v(t)|^2. \quad (14)$$

In this paper, we ignore $\Gamma_{\text{cav}}^{(NR)}$ and Eq. (14) represents the combined transmission spectrum.

C. Disorder and intermolecular couplings

Disorder can be implemented in the Hamiltonian (1) and (9) by assuming that either the molecular transition energies E_m or the molecular coupling with its radiative environment [V_{m0} in Eq. (3) or V_{mv} in Eq. (11)] have a random component. This random component can be constant in time (static disorder) or time dependent (dynamic disorder).

1. Energy disorder

If we focus first on molecular transition energy disorder, the static disorder limit is described by including a random component in the individual molecular frequencies ($\omega_m = E_m/\hbar$)

$$\omega_m = \omega_c + \Omega_m. \quad (15)$$

Here, ω_c is the resonant frequency between molecular ground state $|0\rangle$ and $|m\rangle$ (without disorder). In the calculations reported below, the random component Ω_m is sampled from a Gaussian distribution

$$P(\Omega_m) = \frac{1}{\sqrt{2\pi}\sigma^2} \exp(-\Omega_m^2/2\sigma^2), \quad (16)$$

where different molecules are assumed to be uncorrelated, $\langle \Omega_m \Omega_{m'} \rangle = \delta_{mm'} \sigma^2$, and here the variance σ^2 indicates the disorder strength. This static disorder model may be viewed as the static limit of Kubo's stochastic modulation model where

$$\omega_m = \omega_c + \Omega_m(t) \quad (17)$$

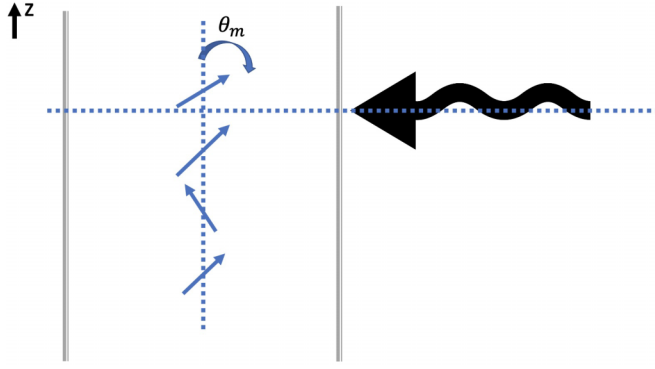


FIG. 1. Schematic diagram of the molecular emitters [blue (gray) arrows] confined in an optical cavity (gray walls) and pumped by the incoming cw field (black line). The field of the cavity mode is assumed to be in the z direction. The transition dipole moments of the emitters have different angles θ_m with respect to the z axis.

and $\Omega_m(t)$ are stochastic random variables that change over time. We choose $\Omega_m(t)$ to be a Gaussian stochastic variable that satisfies $\langle \Omega_m(t) \rangle = 0$ and

$$\langle \Omega_m(t_1) \Omega_{m'}(t_2) \rangle = \delta_{mm'} \sigma^2 e^{-|t_1 - t_2|/\tau_c}, \quad (18)$$

where $\delta_{mm'}$ is a Kronecker delta function. The Gaussian stochastic variables are characterized by the amplitude $\sigma = \langle \delta \Omega^2 \rangle^{1/2}$ and correlation lifetime τ_c of local energy fluctuations. For a detailed algorithm to generate such a stochastic process, see Appendix A.

2. Orientational disorder

The most obvious source of coupling disorder is the inherent orientational disorder that characterizes most molecular liquids, and here we focus on this aspect of our systems. The simplest way to model such disorder is to assign an angle θ_m for each emitter m , where θ_m is oriented with respect to the cavity mode (see Fig. 1). We assume that the field of the cavity mode that may be excited by the external pumping is polarized in the z direction and denote by θ_m the angle between the z axis and the molecular transition dipole direction. This disorder leads to three modifications of the model Hamiltonian. First, the cavity-molecule coupling becomes

$$\hat{V}_{\text{cav-mol}} = \sum_m V_{vm} \cos(\theta_m) |v\rangle \langle m| + V_{mv} \cos(\theta_m) |m\rangle \langle v|. \quad (19)$$

Similarly, for the case outside the cavity, the couplings to the external driving em field also depend on the emitters orientation

$$\begin{aligned} \hat{V}_{\text{pump}} &= \sum_m V_{0m} \cos(\theta_m) \cos(\omega t) |0\rangle \langle m| \\ &+ V_{m0} \cos(\theta_m) \cos(\omega t) |m\rangle \langle 0|. \end{aligned} \quad (20)$$

Also, outside the cavity, the elements of the non-Hermitian \hat{Q} matrix depend on the relative angle $\cos(\theta_m - \theta_{m'})$ [61],

$$\hat{Q} = \sum_{m,m'} \cos(\theta_m - \theta_{m'}) |m\rangle \langle m'|. \quad (21)$$

The disorder of $\{\theta_m\}$ can be either static or dynamic as described in Sec. II C. At room temperature, the charac-

teristic timescale of the rotational motion in solution is of order 10 ps, which implies that in most situations including the light-matter strong-coupling regime in the molecular system, orientational disorder may be assumed static. Nevertheless, for completeness, we will consider below a full range of dynamic disorder. In the static case, we choose a time-independent $\{\theta_m\}$ according to random orientation angles sampled from a Gaussian distribution

$$P(\theta_m) = \frac{1}{\sqrt{2\pi}\sigma^2} \exp(-\theta_m^2/2\sigma^2). \quad (22)$$

This again is the limit $\tau_c \rightarrow \infty$ of a process where orientations are dynamically modulated according to $\langle \theta_m(t) \rangle = 0$ and

$$\langle \theta_m(t_1) \theta_{m'}(t_2) \rangle = \delta_{mm'} \sigma^2 e^{-|t_1 - t_2|/\tau_c}. \quad (23)$$

3. Orientational disorder with intermolecular coupling

To complete our investigation of the linear response of molecules outside and inside optical cavities as expressed by the absorption and transmission signals, we will also consider models with intermolecular couplings (dipole-dipole couplings), again focusing on static and dynamic orientational disorder. The intermolecular coupling is modeled by a dipole-dipole coupling

$$\begin{aligned} \hat{V}_{\text{dip}} &= \sum_{m=k+1}^N \sum_{k=1}^n W_k f(\theta_m, \theta_{m-k}) |m\rangle \langle m-k| \\ &+ \sum_{m=k+1}^N \sum_{k=1}^n f(\theta_{m-k}, \theta_m) W_k |m-k\rangle \langle m|. \end{aligned} \quad (24)$$

Here $W_k = W/k^3$ and in the calculations reported below we use $W = 0.1$ [62], unless specified otherwise. In principle, this Hamiltonian describes a chain of emitters and the interaction between them decays as one over their distance cubed $1/r^3$, as sketched in Fig. 1.

The function $f(\theta_m, \theta_{m-k})$ in Eq. (24) reflects the angular dependence of the dipole-dipole coupling between emitters and is given by

$$f(\theta_m, \theta_{m-k}) = \cos(\theta_m - \theta_{m-k}) - 3 \cos \theta_m \cos \theta_{m-k}. \quad (25)$$

Again, these angles are defined to be relative to the polarization of the incoming driving electric field.

D. Steady-state flux

In order to simulate cavity-molecular dynamics, we propagate the Schrödinger equation for the Hamiltonians above under steady-state boundary conditions. The wave function for the driven, open quantum system can be written as $|\Psi\rangle = c_0|0\rangle + c_v|v\rangle + \sum_m c_m|m\rangle$. This implies propagating the Schrödinger equation $i\hbar \frac{d}{dt} |\Psi\rangle = \hat{H} |\Psi\rangle$ under the Hamiltonians of Eqs. (1) and (9) keeping $|c_0|^2 = 1$. The long-time evolution yields the steady-state forms of the coefficients $c_m(t)$ and $c_v(t)$ that are used to evaluate the steady-state fluxes J_{rad} [Eq. (7)], J_{loc} [Eq. (8)], and J_{cav} [Eq. (14)]. Again, the total steady-state flux $J_{\text{rad}} + J_{\text{loc}}$ as a function of the incoming driving frequency yields the steady-state absorption spectrum for emitters outside optical cavities, while inside the cavity, the steady-state flux J_{cav} gives the reflection or transmission spectrum and J_{loc} represents the local relaxation flux. All

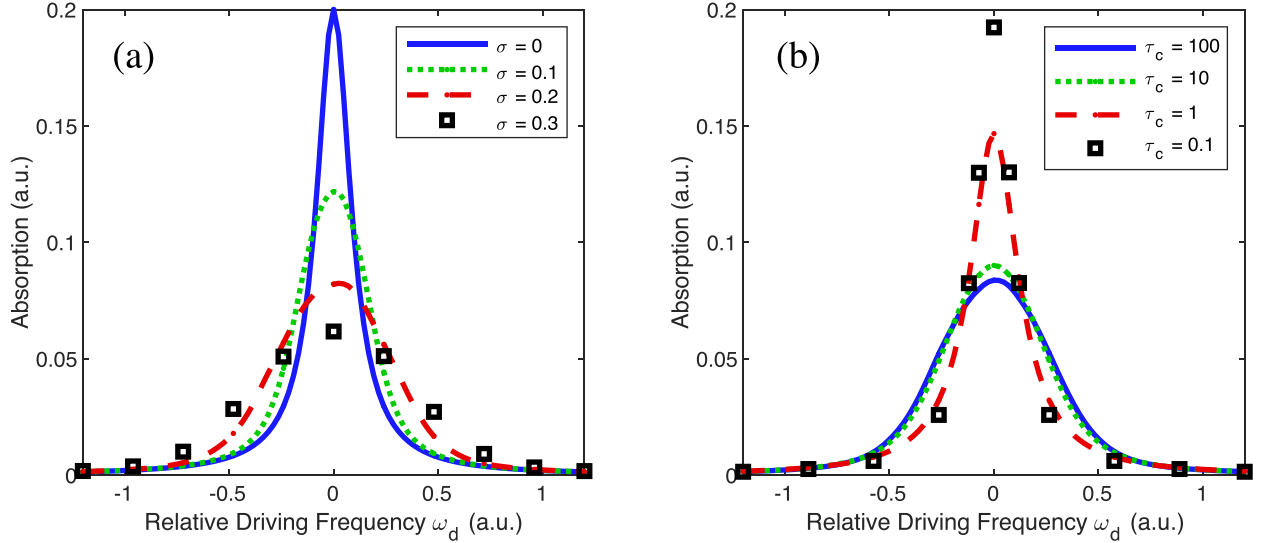


FIG. 2. Steady-state absorption spectra for a molecular ensemble outside the cavity with (a) different static energetic disorder strengths and (b) different correlation times τ_c but constant disorder strength $\sigma = 0.2$. The molecular ensemble includes $N = 40$ molecules. If there is no disorder [(a) $\sigma = 0$, blue (dark gray) solid line], the linewidth of the peak is $2N\Gamma_{\text{rad}} + 2\Gamma_{\text{loc}}$. As the static disorder strength increases, we obtain a broader inhomogeneous peak. As the correlation time decreases under fixed disorder strength [(b) $\sigma = 0.2$], the peak gets narrower, reflecting motional narrowing. As shown in Eqs. (26) and (27), as well as Appendix B, these features can be explained analytically.

results (for systems with both static and dynamic disorder) were conducted by sampling over 256 realizations for each form of disorder and averaging over realizations. We have verified that this procedure was sufficient to render converged results.

With this single-exciton model, there are many parameters we can adjust to account for different physical conditions. We list all symbols and explain our choices of values for these parameters in Appendix E. We will discuss these different possibilities in the following sections.

III. RESULTS

A. Energy disorder

In Fig. 2 we plot the absorption spectrum for an ensemble of emitters outside the cavity. In the limit of zero disorder, the linewidth of the absorption spectrum is associated with the decay rate for the radiative and local nonradiative channels. For the static disorder results [Fig. 2(a)], as the disorder strength σ increases, the absorption line shape become lower and broader. This feature reflects inhomogeneous broadening and the static uncertainty in the molecular excitation energy. Under dynamic disorder [Fig. 2(b)], as the correlation time τ_c decreases, the absorption linewidth is smaller, which reflects motional narrowing. We can also predict the absorption line shape in Fig. 2 using Kubo's stochastic theory of the line shape [63–65]. By performing a Fourier transform of the normalized correlation function $\phi(t)$, we obtain

$$\phi(t) = \exp \left[-\sigma^2 \tau_c^2 (t/\tau_c - 1 + e^{-t/\tau_c}) - (N\Gamma_{\text{rad}} + \Gamma_{\text{loc}})t \right]. \quad (26)$$

For the case of static disorder ($\tau_c \rightarrow \infty$), we can simplify the formula by expanding the exponential of t/τ_c ,

$$\phi(t) \rightarrow \exp[-\sigma^2 t^2/2 - (N\Gamma_{\text{rad}} + \Gamma_{\text{loc}})t], \quad (27)$$

which, after a Fourier transform, yields a convolution between the Gaussian associated with static disorder and the Lorentzian associated with the radiative and nonradiative decay rates. For more details and a comparison of analytic versus numerical results, see Appendix B.

Next consider the case where the same ensemble of emitters interacts with a single-mode cavity under steady-state pumping. As discussed in Sec. II B, we calculate two observables: the steady-state flux J_{cav} through the cavity leakage channel (which gives the combined transmission spectrum) and the steady-state flux J_{loc} through the local relaxation channel of individual emitters. The results in Fig. 3 show that static disorder leads to an inhomogeneous broadening of the two polariton peaks that are present in both of the relevant channels. Interestingly, Fig. 4, in which we suppress the homogeneous contributions (i.e., when non-Hermitian parts Γ_{rad} , Γ_{loc} , and Γ_{cav} are small) to the line shape so that the width is dominated by the inhomogeneous contribution, shows that this inhomogeneous broadening is much weaker inside a cavity relative to outside a cavity. This effect has already been seen in Ref. [66].

Returning to Fig. 3, we note that, for increasing σ , the baseline between the two polariton peaks (around relative driving frequency $\omega_d = \omega - \omega_c$) for the local relaxation channel becomes larger, whereas in the transmission spectrum, the baseline around relative driving frequency $\omega_d = 0$ remains approximately zero. This different behavior arises because the dark modes cannot contribute to the transmission spectrum but they do contribute to the local relaxation channel. Another observation in Figs. 3(a) and 3(b) is the increase of the effective Rabi splitting as the energetic static disorder strength increases. This increase can be captured approximately by the formula

$$\Omega_R(\sigma)/\Omega_R(\sigma = 0) = 1 + 2\sigma^2/\Omega_R(\sigma = 0)^2. \quad (28)$$

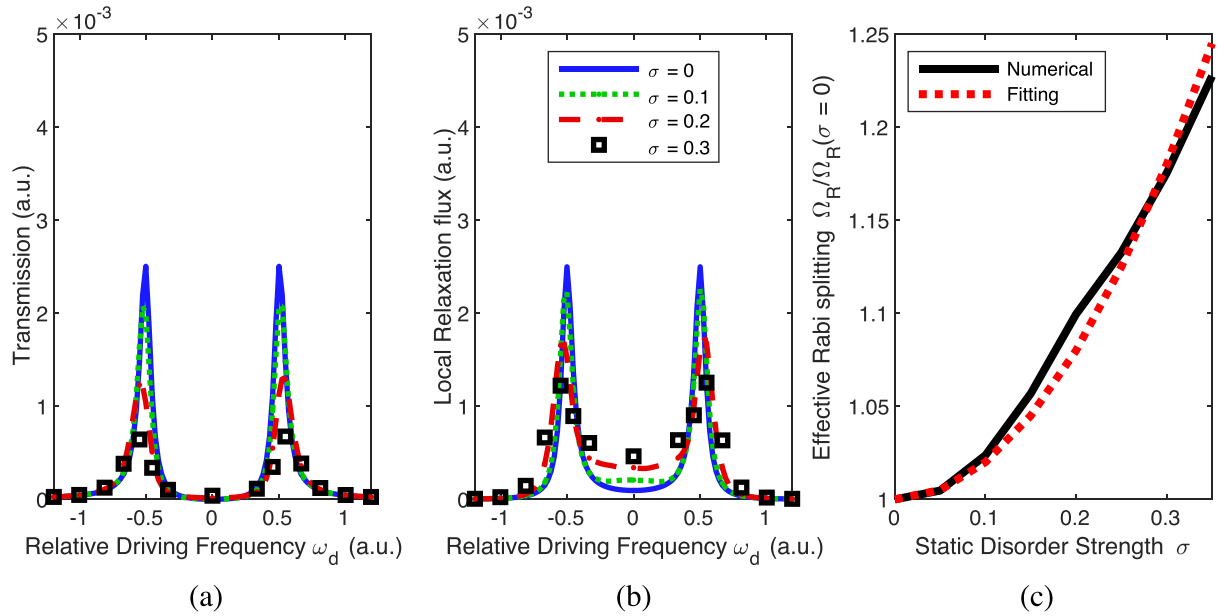


FIG. 3. Steady-state (a) transmission and (b) local relaxation flux spectra, as calculated for molecular ensembles with different static energetic disorder strengths σ interacting with a single-mode cavity. The molecular ensemble and the cavity mode form two polariton peaks in both figures. As the amplitude of static disorder increases, the split peaks become broadened; however, the baseline in between the two peaks (around relative driving frequency $\omega_d = 0$) grows larger only for the local signal. This growth arises because the dark modes contribute only to the local relaxation flux but not to the transmission spectrum. Finally, note that as the energetic static disorder increases, the effective Rabi splitting increases. This increase can be captured approximately by perturbation theory [Eq. (28)].

One can obtain such a formula by using second-order perturbation theory for the polariton states. For a simple derivation, see Appendix C.

Finally, for the case with dynamic disorder, as shown in Fig. 5, as one might expect, we find motional narrowing for

both channels as the correlation time τ_c decreases (similar to Fig. 2). Moreover, we observe the same behavior as in Fig. 3: In between the two polariton peaks (around relative driving frequency $\omega_d = 0$), the presence of dark modes leads to a finite steady-state flux for the local relaxation channel.

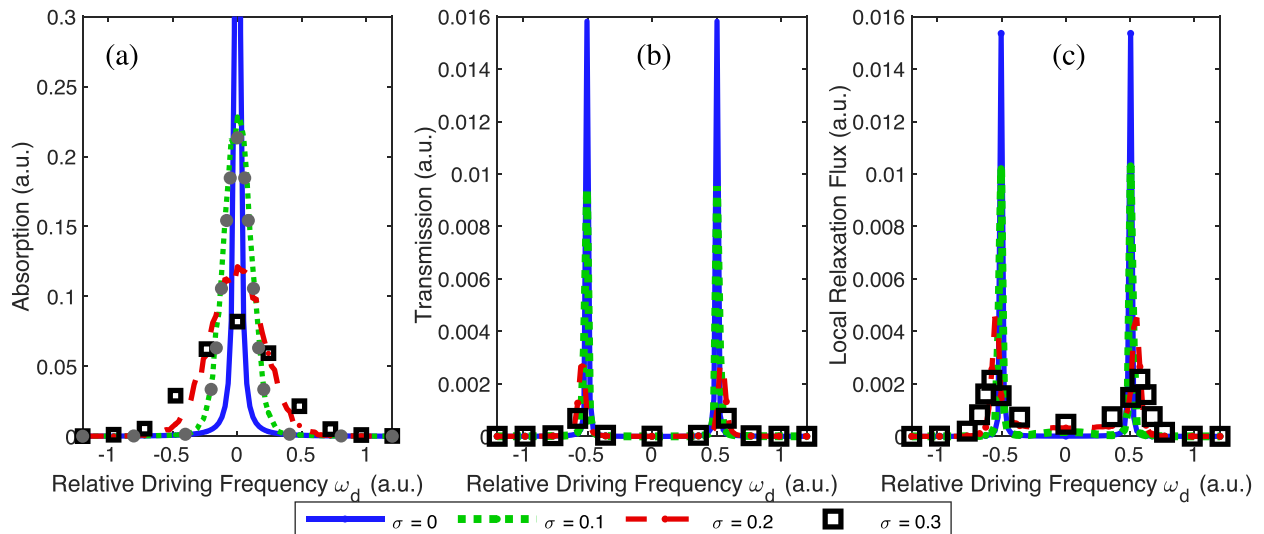


FIG. 4. Steady-state (a) absorption spectra for outside the cavity, (b),(c) transmission and local relaxation flux spectra interacting with a single-mode cavity, as calculated for molecular ensembles with different static energy disorder strengths σ . The gray dots in (a) are analytical results calculated in Appendix B. Here the contributions to homogeneous broadening, namely, the non-Hermitian parts of the Hamiltonian matrices, are taken to be $\Gamma_{\text{rad}} = 0.005/N$, $\Gamma_{\text{cav}} = 0.005$, and $\Gamma_{\text{loc}} = 0.005$, which are ten times smaller than in Fig. 3, so (except from the case without disorder) the linewidth outside the cavity is dominated by the inhomogeneous broadening. In agreement with earlier observations [66], the inhomogeneous broadening observed outside the cavity is not manifested in the linewidth of the polariton peaks inside the cavity, which are therefore much narrower, as seen in (b) and (c).

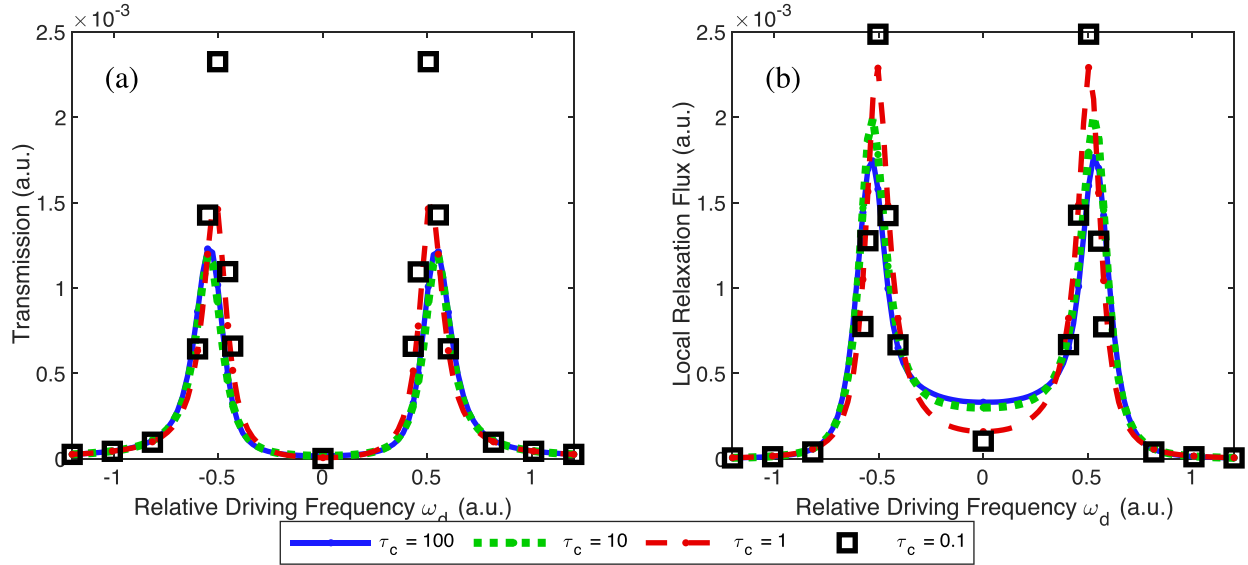


FIG. 5. Steady-state (a) transmission spectra and (b) local relaxation flux for the molecular ensemble inside a single-mode cavity with dynamic disorder. We fix the energy disorder strength ($\sigma = 0.2$) and scan the correlation times $\tau_c = 100, 10, 1, 0.1$. The molecular ensemble and the cavity mode forms two polariton peaks in both figures. Note that the long correlation limit (blue solid lines) recovers the results with static disorder in Fig. 3 (red dashed lines). Note also that, similar to Fig. 3, the dark modes contribute only to the local relaxation channel. As we decrease τ_c , the two peaks become narrower in both figures and the dark modes contribute less to the local relaxation channel.

B. Orientational disorder

In this section we present results for angular disorder as defined in Sec. II C 2. Note that the way disorder is defined in this case implies the average contribution is nonzero ($\langle |\cos \theta_m| \rangle \neq 0$) and therefore some of the results shown below reflect this situation. As shown in Fig. 6, for the static angular disorder case, as the disorder strength σ increases, both the height and the linewidth of the absorption peak decrease [see Eq. (22)]. This decrease arises because each dipole in the ensemble of emitters couples to the driving field differently, resulting in less collective behavior. For the

dynamic angular disorder case, in agreement with the results in Sec. III A, as we decrease the correlation time of the angular disorder, we find motional narrowing.

Next we consider this molecular ensemble with angular disorder inside the cavity. The results are shown in Fig. 7. Unlike the results in Fig. 3 (where we investigated disorder in the excitation energies), here the Rabi splitting consistently decreases as we increase the static angular disorder strength and lose collectivity of the response. Clearly, when interpreting the spectra from the cavity, one must consider geometry and not just the energy levels of the molecules in the

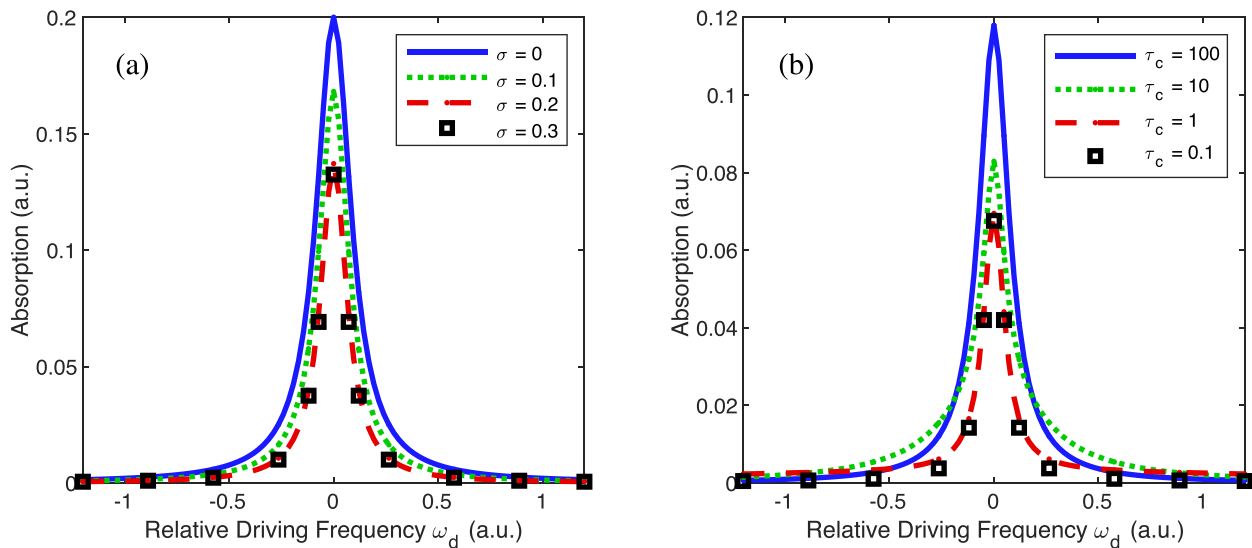


FIG. 6. Steady-state absorption spectra for the ensemble of emitters outside the cavity: (a) static angular disorder and (b) dynamic angular disorder. As shown in (a), when the disorder strength σ increases, the absorption peaks decrease. More importantly, the linewidth decreases because the emitters act less collectively. For the case of dynamic disorder in (b), similar to Fig. 2, we observe motional narrowing.

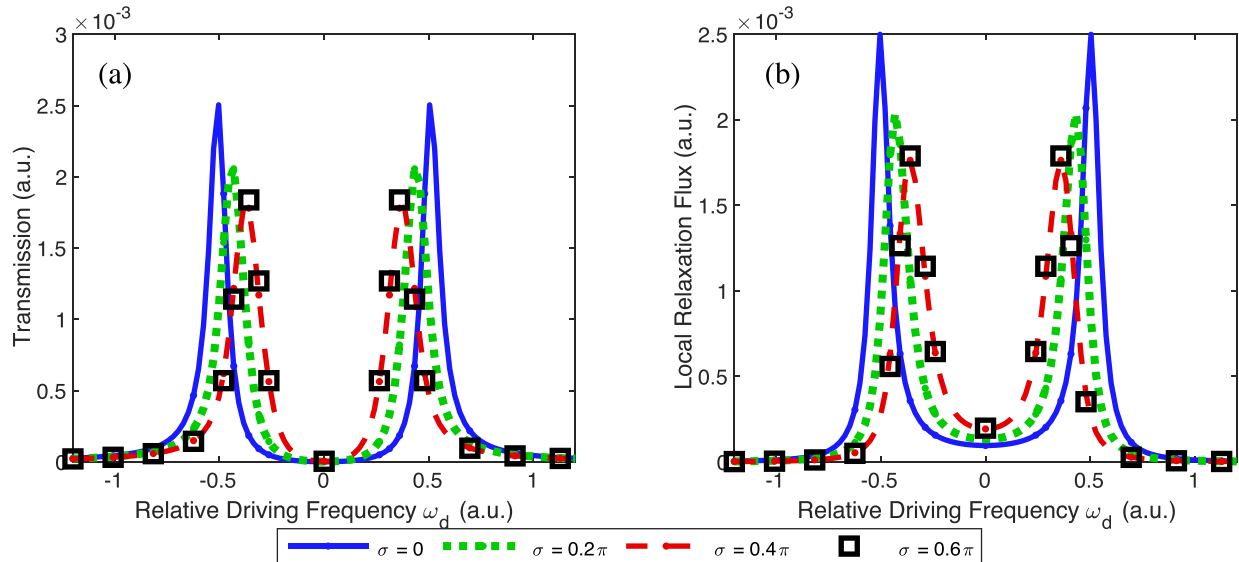


FIG. 7. Steady-state (a) transmission spectra and (b) local relaxation flux for different static angular disorder strengths ($\sigma = 0, 0.2\pi, 0.4\pi, 0.6\pi$) inside a cavity. As shown in the figures, when the disorder strength σ increases, the absorption peak height decreases and the dark modes contribute only to the local relaxation flux but not to the transmission spectrum (similar to Fig. 3). However, unlike Fig. 3, disorder in the angles leads to a decrease in the Rabi splitting.

cavity. In principle, in a cavity, one might expect to have both energy and angular disorder and so, as the temperature rises, the Rabi splitting should decrease. Unfortunately, it remains unclear which effect dominates. Note that the increase of Rabi splitting with increasing static energy disorder does not suggest that more emitters are behaving collectively. As shown in both Figs. 3 and 7, the maximal radiative steady-state flux decreases as static disorder strength σ increases. Finally, as in Fig. 3, the dark modes contribute to the rise of the baseline between the two polariton peaks only for the local relaxation channel.

The results for the dynamic angular disorder case are slightly more nonintuitive. In Fig. 8 we fix the disorder strength ($\sigma = 0.4\pi$) and calculate transmission and local relaxation fluxes for different correlation times τ_c . In the long correlation time limit (blue solid line), we recover the static disorder result. Two features are worth noting in Fig. 8. First, as τ_c becomes smaller, we find that, as expected, the polaritonic spectra undergo motional narrowing. However, reducing the correlation time is not equivalent to reducing disorder insofar as the Rabi splitting in Fig. 8 decreases as $\tau_c \rightarrow 0$ (whereas the Rabi splitting increases as $\sigma \rightarrow 0$ in Fig. 7),

$$E_{\text{LRUP}} = \pm \sqrt{N|V_{mv}|^2 \langle |\cos(\theta_m)|^2 \rangle}. \quad (29)$$

Here angular brackets stand for an ensemble average. For the no-correlation limit ($\tau_c = 0$), a good estimate is

$$E_{\text{LRUP}} = \pm \sqrt{N|V_{mv}|^2 \langle |\cos(\theta_m)| \rangle}. \quad (30)$$

However, we are unable to predict what Rabi splittings are for finite τ_c . For detailed derivations of these expressions and an analysis of how they match up with numerical results, see Appendix D. Note that in both limits, the Rabi splittings are smaller than the case with no disorder, reflecting the fact that the average coupling in this model is smaller than V_{mv} .

Another nonintuitive result in Fig. 8 pertains to the height of the peaks themselves. Here we see that the height behaves in a nonmonotonic fashion as a function of τ_c ; starting from static disorder and decreasing τ_c , we find that the peak height and integral decrease and then increase. Qualitatively, we believe this nonmonotonic behavior can be understood by recognizing that with moderate correlation times, introducing disorder and slowly distorting the coherences removes the possibility of seeing individual configurations, each absorbing for a long time, or seeing many configurations averaged to one static configuration. As a result, there is less absorption at intermediate correlation times. Pursuing a more rigorous analysis of this effect will certainly be an important research direction in the future. Finally, just as in Fig. 7, the dark modes contribute to the local relaxation, and as the correlation time decreases, the Rabi splitting decreases.

C. Intermolecular coupling and orientational disorder

Finally, let us address the presence of how intermolecular coupling affects orientational disorder. Let $|B\rangle$ be the bright state of the system outside the cavity, which is defined by applying the transition dipole moment operator to the total ground state $|0\rangle$:

$$|B\rangle = \frac{\hat{\mu}|0\rangle}{|\hat{\mu}|0\rangle} = \frac{1}{\sum_j \cos^2 \theta_j} (\cos \theta_1, \cos \theta_2, \dots)^T. \quad (31)$$

Before presenting the absorption spectra, we start by showing the density of states of the system outside or inside a cavity, weighted by the brightness of the states in Fig. 9. For the case outside the cavity, we define the brightness W_j of each eigenstate ϕ_j of \hat{H}_{sub} (keeping only the real part of m and v elements [see Eqs. (C1)–(C3) in Appendix C]) to be

$$w_j = |\langle B|\phi_j\rangle|^2. \quad (32)$$

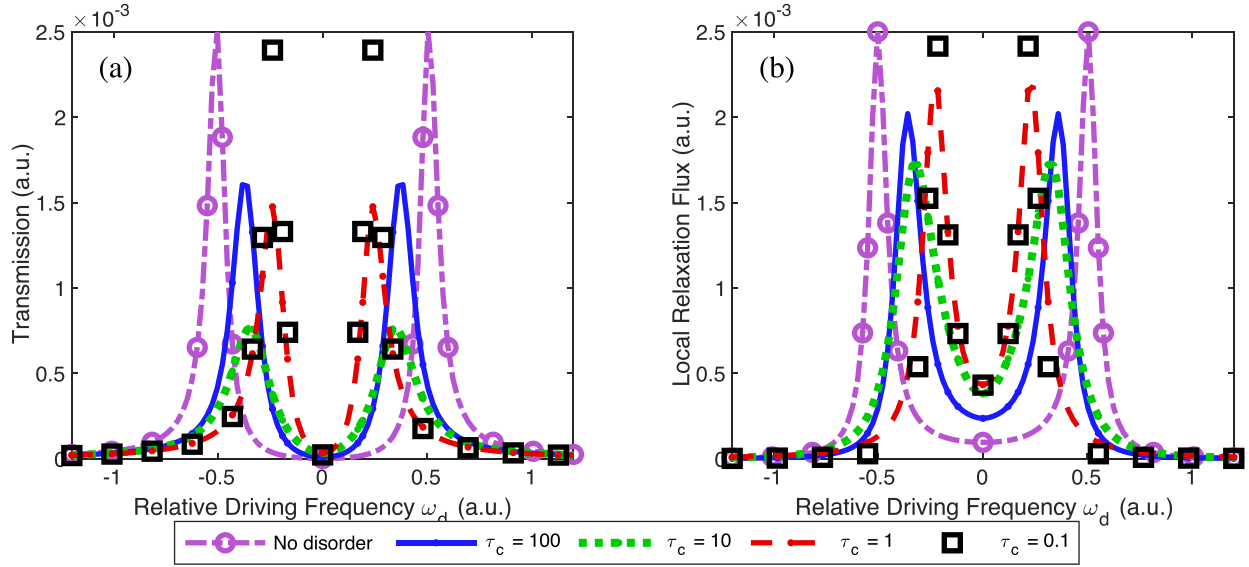


FIG. 8. Steady-state spectra for dynamic angular disorder in a single-mode cavity: (a) transmission and (b) local relaxation flux. We fix the angular disorder strength ($\sigma = 0.4\pi$) and scan over correlation times $\tau_c = 100, 10, 1, 0.1$. We also plot the result with no disorder for reference (purple dash-dotted line with circles). As shown in both figures, when the correlation time decreases, the collective effect diminishes, leading to a smaller Rabi splitting. Similar to Fig. 7, the dark modes contribute only to the local relaxation signals.

For the case inside the cavity, the bright mode must contain the cavity mode and thus the following definition makes more sense:

$$w_j^{\text{cav}} = |\langle v | \phi_j \rangle|^2. \quad (33)$$

Here $|v\rangle$ is the bare cavity state [see Eqs. (9)–(13)]. As shown in Fig. 9, for the case outside the cavity, the brightest eigenstates have negative energy eigenvalues (relative to the emitters energy). For the case inside the cavity, there are two regions of bright states corresponding to the two polariton

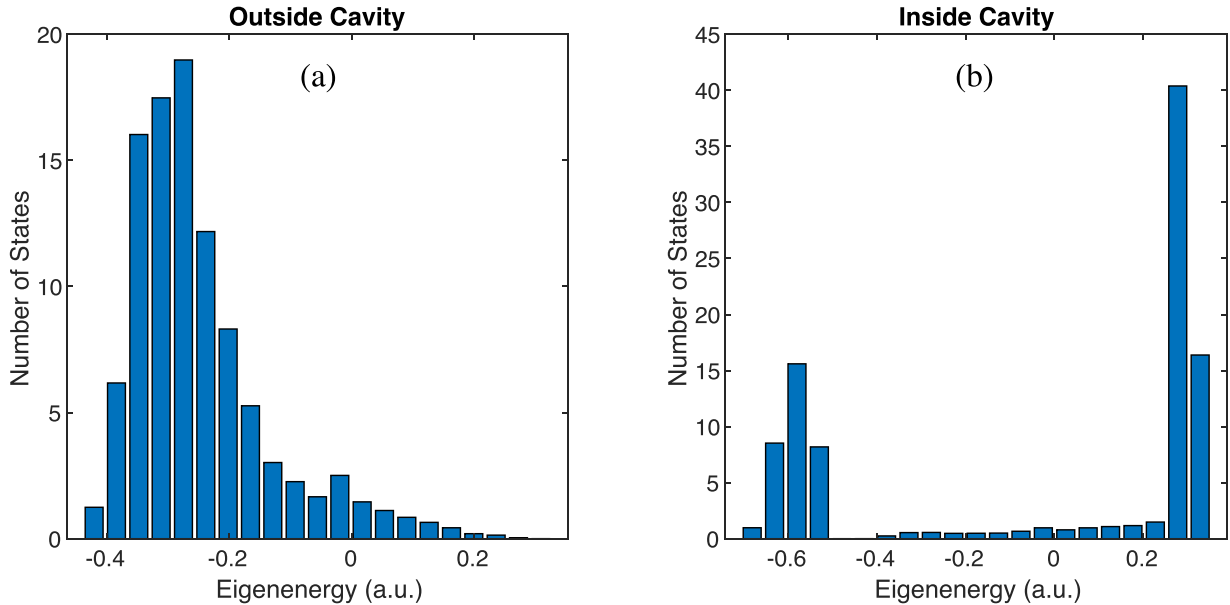


FIG. 9. Histogram of the brightness [w_j in Eq. (32) and w_j^{cav} in Eq. (33)] for the Hamiltonian eigenstates that arise with intermolecular coupling [see Eqs. (24) and (25)] as averaged over realizations of θ_m following the distribution in Eqs. (22) and (23). These brightness factors are relevant to pumping the emitters (a) outside and (b) inside the cavity. We consider that the dipoles are fully aligned in the limit of zero disorder and thus intermolecular couplings are negative [Eq. (25) equals -2]. The eigenvalue of the bright state (symmetric superposition state) becomes negative. Hence, for the case outside the cavity, the brightest states have energy $E \approx -0.3$ a.u., which is lower than the energy of the independent emitters (which is set to be 0); for the case inside the cavity, the two brightest states yield lower and upper polariton peaks at around $E = -0.6$ and 0.3 a.u., respectively. The upper polariton peak is brighter than the lower polariton because the former has an energy eigenvalue (0.3 a.u.) closer to the energy of the bare cavity mode (0 a.u.). Again, the center of the two polariton peaks [$(E_{\text{LP}} + E_{\text{UP}})/2 \approx -0.15$ a.u.] is lower than the energy of the independent emitters or bare cavity mode.

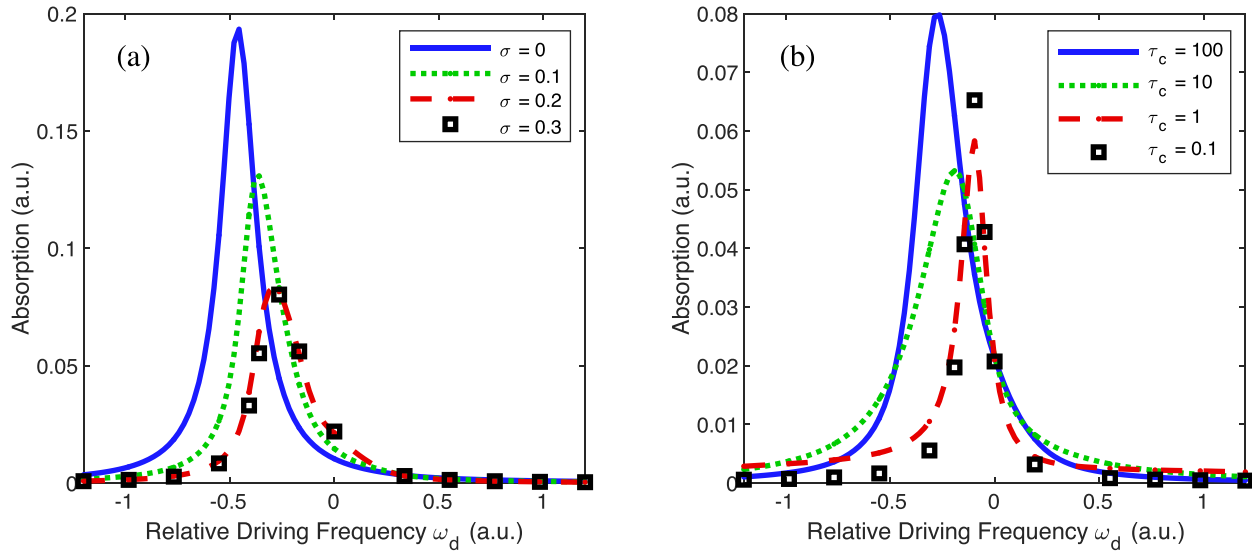


FIG. 10. Steady-state absorption for emitters outside a cavity with intermolecular couplings and (a) static orientational disorder and (b) dynamic orientational disorder. (a) For the static disorder case, the absorption peaks height decreases as the disorder strength increases. As predicted in Fig. 9, intermolecular coupling reduces the energy of the system and the peaks appear to have energy lower than that of the individual emitters. (b) For the dynamic disorder case, the peak gets narrower as we decrease the correlation time.

peaks; the center of the two peaks is shifted towards the negative direction, just as for the case outside the cavity. The upper polariton eigenstates are brighter than the lower polariton because they are closer to the bare cavity mode energy.

With these structures in mind, in Fig. 10 we plot the absorption spectra for different orientational disorder strengths. When there is no orientational disorder, because there is finite negative intermolecular coupling, the peaks are redshifted, as the brightest eigenstate corresponds to the smallest eigenvalue. As we increase the disorder strength, the total absorption decreases. For the dynamic orientational disorder case, similar to Fig. 6, as the correlation time decreases, the absorption linewidth decreases (corresponding to motional narrowing). The scale of the redshift is also reduced as we increase modulation speed.

In Fig. 11 we plot the transmission and local relaxation flux for an ensemble of emitters placed inside the cavity. First, one might guess from what was shown in Fig. 9 that the upper polariton peak height is greater than that of the lower polariton; the center of the two polariton peaks has a lower energy than that of the bare cavity mode. Second, as the static disorder strength increases, the effective Rabi splitting decreases because the disorder reduces the collectiveness of the emitters. Moreover, the center of two polariton peaks becomes closer to the origin. In the limit of infinite disorder, we recover a uniform distribution of angles as in a homogeneous two-dimensional system. Third, as we compare the two channels, because the transmission spectrum relies on the cavity mode and the local relaxation relies on the emitter states, the difference in intensity between the upper and lower polaritons for the transmission spectrum is greater than that for the local relaxation signals. Finally, the dark modes contribute only to the local relaxation signals, as was also seen in Fig. 7.

Finally, we show the steady-state transmission and local relaxation flux inside a single-mode cavity with intermolecular coupling and dynamic orientational disorder in Fig. 12. As the

correlation time decreases, the effective Rabi splitting and the linewidth of each polariton peak decrease, just as in Fig. 8. The difference between the upper and lower polariton peak heights is less significant in local relaxation flux than in the transmission spectrum, similar to what was found in Fig. 11. All the observations are consistent with those in Sec. III B.

IV. CAVITY EFFECT ON LOCAL RELAXATION YIELD

The models defined by Eqs. (1)–(13) are minimal models that allow consideration of three relaxation channels for the radiation absorbed from the driving field: a radiative channel that combines transmission and reflection, nonradiative damping of the cavity mode (heat production in the cavity walls), and reactive relaxation. The latter represents a reaction that occurs following the molecular excitation. It is of interest to examine the effect of the cavity environment on the yield of the latter channel.

Outside the cavity, the system undergoes collective super-radiance at a rate $N\Gamma_{\text{rad}}$ and local relaxation at a rate Γ_{loc} . The yield Y of the individual molecular relaxation (which we assume to be a reactive process) is

$$Y = \frac{\Gamma_{\text{loc}}}{N\Gamma_{\text{rad}} + \Gamma_{\text{loc}}}. \quad (34)$$

By comparison, inside the cavity, the energy will leak through the cavity mode at rate Γ_{cav} with the same local relaxation rate as above, Γ_{loc} . It is clear that the local yield is then

$$Y = \frac{\Gamma_{\text{loc}}}{\Gamma_{\text{cav}} + \Gamma_{\text{loc}}}. \quad (35)$$

Hence, without disorder, we can expect that the reactive relaxation yields will be different outside and inside the cavity, in terms of both absolute value and N dependence. This difference is shown in Fig. 13. Note that, for simplicity, we assume $\Gamma_{\text{cav}} = 10\Gamma_{\text{rad}}$. In agreement with Eqs. (34) and (35), the local

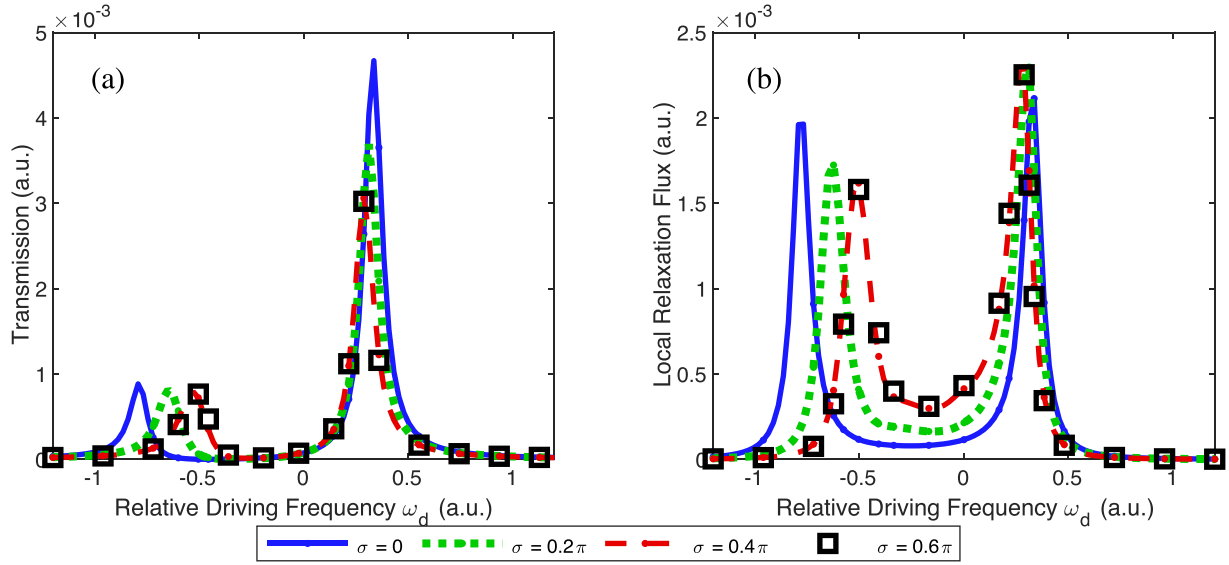


FIG. 11. Steady-state (a) transmission and (b) local relaxation for an ensemble of emitters inside a single-mode cavity with intermolecular couplings for different static orientational disorder strength. As predicted in Fig. 9, the upper polariton contributes more strongly than does the lower polariton peak to the transmission spectrum. Intermolecular couplings stabilize the system and thus the center of the two polariton peaks corresponds to an energy lower than that of an individual emitter or bare cavity mode. As the disorder strength increases, the Rabi splitting decreases as the collectiveness is destroyed by the disorder. The difference in height between the upper and lower polariton peaks is small for the local relaxation channel because the signals are not dependent on how strong the cavity mode contribution to the polariton is (but rather are dictated by the dynamics of the individual emitters).

relaxation yield depends on N only when the emitters are outside the cavity.

Consider now the effect of disorder. As discussed above and shown in Figs. 2 and 5, at reasonably high temperatures, nuclear motion and dephasing processes lead to static and dynamic disorder, which results in a reduction of steady-state

radiative fluxes. As shown in Fig. 13, we can clearly see that moderate dynamic disorder leads to a reduction of radiative fluxes and thus a greater local relaxation yield both inside and outside the cavity. More importantly, the slope of the ratio between radiative and local relaxation flux [red dashed line in Fig. 13(a)] is reduced in the presence of disorder

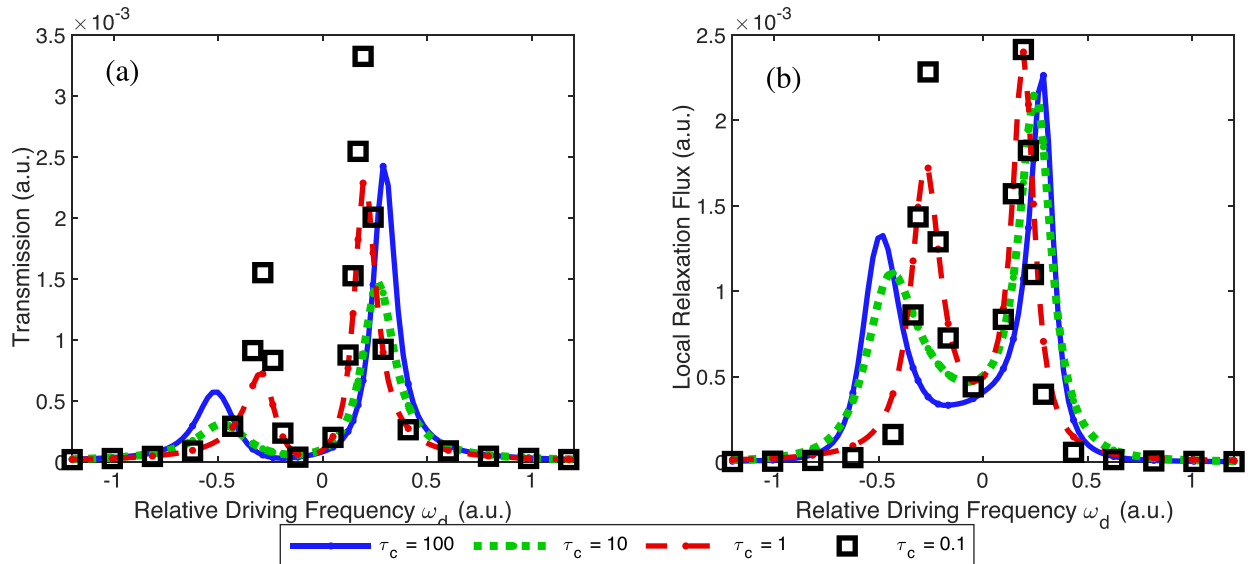


FIG. 12. Steady-state (a) transmission and (b) local relaxation flux for an ensemble of emitters inside the cavity with intermolecular couplings and dynamic orientational disorder. Both figures are for the indicated correlation times but a fixed disorder strength ($\Delta = 0.4\pi$). Again, the long correlation time limit (blue solid lines) is equivalent to static disorder results (red dashed lines in Fig. 11). Both the Rabi splitting and the linewidth decrease as the correlation time decreases, similar to Fig. 8. The center of the two polariton peaks shift to lower energy by the intermolecular coupling. As in Fig. 11, the difference in height between the upper and lower polariton peaks is more significant in the transmission spectrum than in the local relaxation signal.

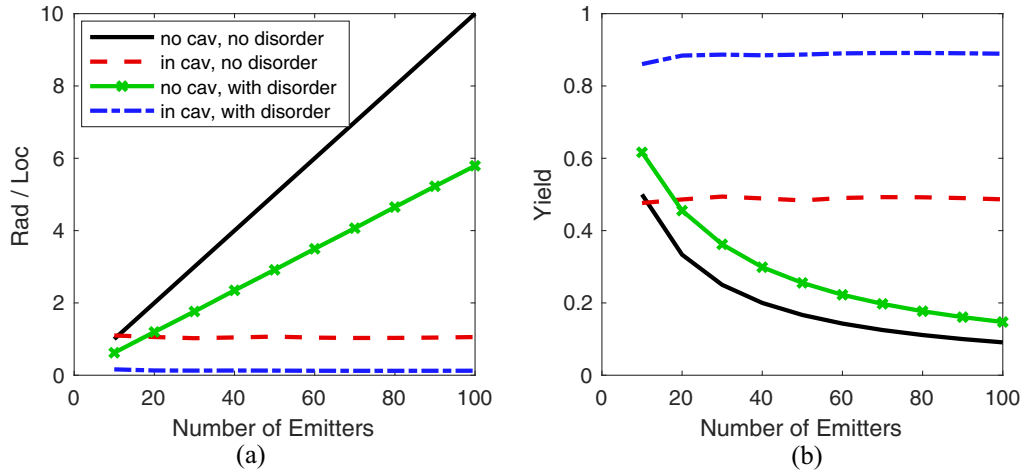


FIG. 13. (a) Steady-state ratio between radiative flux and local relaxation flux outside and inside the cavity with and without energy dynamic disorder. (b) Steady-state local relaxation yield outside and inside cavity with and without energy dynamic disorder. We keep all parameters constant and vary only the number of emitters of the system. We assign the cavity leakage rate to be the same as the local relaxation rate for the case of the system inside the cavity. For the case without disorder, we choose the superradiant rate for $N = 10$ to be the same as the local relaxation rate for the case outside the cavity. Hence, the local yield at $N = 10$ is 0.5 both inside and outside the cavity. For outside the cavity, as more emitters are collectively emitting, the ratio between the radiative and local relaxation rates increases linearly as N and thus the local yield decreases. For inside the cavity, we assume that the cavity leakage rate remains approximately constant. Hence, the local relaxation yield does not depend on N [24]. From these data, we conclude that adding a single-mode cavity can certainly change the importance of different energy dissipation channels. Now, for the case with moderately fast energetic dynamic disorder ($\sigma = 0.2$ and $\tau_c = 1$), one clear pattern is that for both outside and inside the cavity, the radiative channels are suppressed by the disorder and thus local relaxation yields increase. Moreover, for the case outside the cavity (green line with crosses), the slope decreases from 0.1 (no disorder) to 0.06 (moderate dynamic disorder), which shows that there are 60% emitters behaving collectively. In applying this conclusion to a realistic experiment, note that N should be the effective number of emitters that participate in the superradiant rate or Rabi splitting, which characterizes the collectiveness under the influence of disorder

outside the cavity. In principle, this slope corresponds to the effective number of emitters that contribute to the collective emission. For the parameters in Fig. 13, if we focus on comparing the black solid and red dashed lines, we find a slope of 0.06 for moderate disorder (black dashed line) vs 0.1 for the no-disorder case (blue solid line), which implies that 60% molecules are emitting collectively. However, for very strong dephasing and disorder, we expect that this slope should approach zero and N in Eq. (34) should approach unity; after all, with strong enough dephasing, we expect to find independent spontaneous emission for emitters outside the cavity, in contrast to the superradiant effect in Eq. (34). While this analysis demonstrates a possible cavity effect on the yield of the chemical reaction, a note of caution should be added. This analysis is based on the assumption that Γ_{loc} is identical following excitation of the bright mode outside the cavity, as in the case where a polariton is excited inside the cavity. This is not necessarily the case, because the initially prepared state differs in energy by an amount determined by the Rabi splitting. A model where Γ_{loc} is sensitive to this difference was recently analyzed in Ref. [67].

V. CONCLUSION

We have investigated the influence of energetic disorder, orientational disorder, and intermolecular couplings on the absorption spectra for an ensemble of two-level emitters outside and inside a single-mode cavity. As concerns the influence of energetic and orientational disorder, we recovered

inhomogeneous broadening for static disorder and motional narrowing for dynamic disorder. For the case inside the cavity, there are two inherently different observables: a transmission spectrum and local relaxation flux. The transmission spectrum is dictated primarily by properties of the cavity mode and the local relaxation flux depends mainly on the property of the individual emitters. These two observables are complementary to each other and together provide a comprehensive picture of the system when we introduce different types of disorder. Introducing intermolecular coupling is essentially equivalent to adding finite detuning between the bare cavity mode and the emitters eigenstates. As we compared the two observables, we confirmed that dark modes do not contribute to transmission signals, which require the state to be bright. However, the dark modes do contribute to the local relaxation signals.

Finally, we investigated the differences between excited-state local relaxation yields outside versus inside the cavity. It is clear that the presence of a cavity mode will modify the yield in two ways: changing the radiative energy dissipation rate (from collective spontaneous emission to cavity leakage) and changing inherently how collectiveness translates into physical observables (from superradiance to Rabi splitting) [24].

Looking forward, we note that, in this work, we have assumed that the rate of independent spontaneous emission towards other polarization directions is very slow and can be completely ignored. In truth, however, the influence of other polarization directions cannot really be modeled with a single-mode cavity. To better isolate possible cavity effects

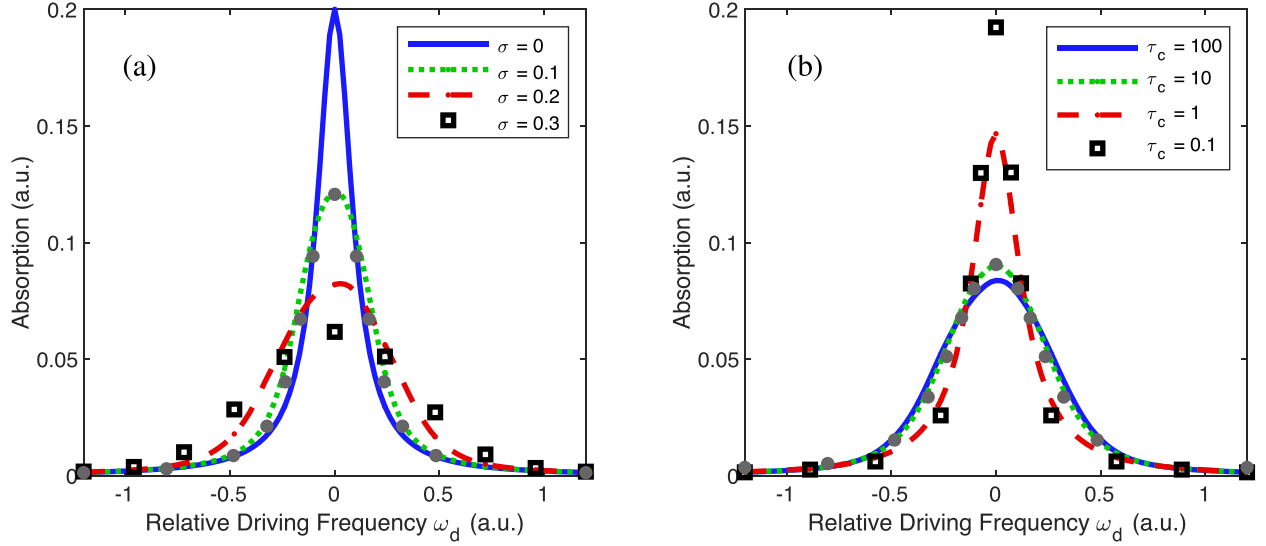


FIG. 14. Steady-state absorption spectra for a molecular ensemble with (a) different static energy disorder strengths and (b) different correlation times τ_c but the same disorder strength $\sigma = 0.2$, identical to Fig. 2. The gray dots are predicted by Eqs. (27) and (26). The linewidths of numerical results match perfectly with the prediction. To avoid crowding the figure, we show only one analytical prediction overlapping with the green dotted lines in both (a) and (b).

in chemistry, one of the next steps would be to incorporate higher dimensions and more cavity modes inside a realistic microcavity (likely through a Maxwell-Bloch calculation).

ACKNOWLEDGMENTS

This work has been supported by the U.S. Department of Energy, Office of Science, Office of Basic Energy Sciences, under Award No. DE-SC0019397 (J.E.S.); the U.S. National Science Foundation under Grant No. CHE1953701 (A.N.).

APPENDIX A: GENERATION OF THE ORNSTEIN-UHLENBECK PROCESS

In our computational procedure, to generate energy modulations, we employ an Ornstein-Uhlenbeck process. To generate a sequence of values at time $t_n = t_0 + ndt$, we sample $\{\Omega_m(t_n)\}$ in the following process [68].

(1) At t_0 , pick $\{\Omega_m(t_0)\}$ according to the Gaussian distribution

$$P[\Omega_m(t_0)] = \frac{1}{\sqrt{2\pi\sigma^2}} \exp\left(-\frac{\Omega_m(t_0)^2}{2\sigma^2}\right).$$

(2) Calculate r_n ,

$$r_n = \exp[-(t_{n+1} - t_n)/\tau_c] = \exp(-dt/\tau_c).$$

(3) Pick $\{\Omega_m(t_{n+1})\}$ according to the conditional probability

$$P[\Omega_m(t_{n+1})|\Omega_m(t_n)] = \frac{1}{\sqrt{2\pi\sigma^2(1-r_n^2)}} \exp\left(-\frac{[\Omega_m(t_{n+1}) - r_n\Omega_m(t_n)]^2}{2\sigma^2(1-r_n^2)}\right).$$

(4) Go back to step 2.

APPENDIX B: VOIGT THEORY

In this Appendix we demonstrate that our numerical results from Sec. III A for the case of a collection of molecules outside the cavity with static or dynamic energetic disorder (Fig. 2) satisfy Voigt theory. According to Eqs. (26) and (27), we can analytically predict the Voigt linewidth for different disorder strengths σ and correlation times τ_c . However, we cannot determine the absolute peak height from Eqs. (26) and (27). Nevertheless, if we simply fit the line shape with the numerical height, then Fig. 14 demonstrates that the analytic linewidths predicted by Eqs. (27) and (26) (gray dots) match perfectly with the numerical linewidths in Fig. 2.

APPENDIX C: DERIVATION OF THE EFFECTIVE RABI SPLITTING UNDER STATIC ENERGETIC DISORDER

In this Appendix we use second-order perturbation theory to derive Eq. (28). The total Hamiltonian of the disordered system is

$$\hat{H}_{\text{sub}} = H_0 + \Lambda, \quad (\text{C1})$$

$$H_0 = E_v|v\rangle\langle v| + \sum_{m=1}^N E_m|m\rangle\langle m| + V_{mv}(|m\rangle\langle v| + |v\rangle\langle m|), \quad (\text{C2})$$

$$\Lambda = \sum_{m=1}^N \delta E_m|m\rangle\langle m|. \quad (\text{C3})$$

Here N is the effective number of emitters in the cavity. The modulation δE_m is treated as perturbation and has zero mean and σ^2 variance. We assume no detuning and thus the Rabi splitting with no disorder is

$$\Omega_R(\sigma = 0) = 2\sqrt{N}V_{mv}. \quad (\text{C4})$$

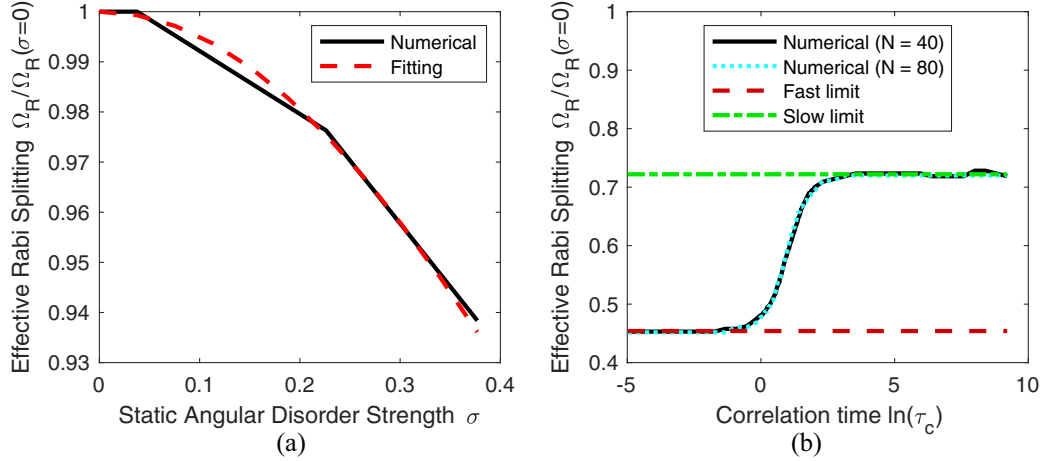


FIG. 15. Effective Rabi splitting vs (a) static angular disorder strength and (b) dynamic angular disorder correlation time. As shown in (a), static angular disorder leads to contraction of Rabi splitting. This contraction is unlike the case with static energetic disorder, in which the effective Rabi splitting increases as the disorder strength increases. The formula (D7) obtained by cumulant expansion captures the contraction of effective Rabi splitting induced by static angular disorder ($\tau_c \rightarrow \infty$). For the case with dynamic angular disorder ($\sigma = 0.4\pi$), as shown by the green dash-dotted line in (b), we can only predict the fast modulation limit $\tau_c = 0$ as in Eq. (D8). For the intermediate correlation time, the effective Rabi splitting is not fully determined by the first and second moments. As shown by the cyan dotted line, the effective Rabi splitting is also independent of N in the system.

The polariton states have energy $\pm\Omega_R(\sigma = 0)/2$ and the corresponding eigenvectors are

$$|\text{UP,LP}\rangle = (1/\sqrt{2}, \pm 1/\sqrt{2N}, \dots, \pm 1/\sqrt{2N}). \quad (\text{C5})$$

All remaining eigenstates are dark states and have energy $E_{\text{dark}} = 0$. Second-order perturbation theory yields the energies of the polariton states

$$E_{\text{LP}} = E_{\text{LP}}^0 + \langle \text{LP} | \Lambda | \text{LP} \rangle + \sum_{k \neq \text{LP}} \frac{|\langle k | \Lambda | \text{LP} \rangle|^2}{E_{\text{LP}}^0 - E_k^0}. \quad (\text{C6})$$

The first-order term is the mean of the static disorder

$$\langle \text{LP} | \Lambda | \text{LP} \rangle = \sum_{m=1}^N \delta E_m / 2N = 0. \quad (\text{C7})$$

The second term is

$$\begin{aligned} & \sum_{k \neq \text{LP}} \frac{|\langle k | \Lambda | \text{LP} \rangle|^2}{E_{\text{LP}}^0 - E_k^0} \\ &= - \frac{\sum_k |\langle k | \Lambda | \text{LP} \rangle|^2 - |\langle \text{LP} | \Lambda | \text{LP} \rangle|^2 - |\langle \text{UP} | \Lambda | \text{LP} \rangle|^2 / 2}{\Omega_R(\sigma_0) / 2}, \end{aligned} \quad (\text{C8})$$

$$\sum_k |\langle k | \Lambda | \text{LP} \rangle|^2 = \langle \text{LP} | \Lambda^2 | \text{LP} \rangle = \sum_{m=1}^N \delta E_m^2 / 2N = \sigma^2 / 2, \quad (\text{C9})$$

$$|\langle \text{UP} | \Lambda | \text{LP} \rangle|^2 / 2 = - \left| \sum_{m=1}^N \delta E_m \right|^2 / 4N = 0. \quad (\text{C10})$$

Hence, the perturbed energy is

$$E_{\text{LP}} = E_{\text{LP}}^0 - \frac{\sigma^2}{\Omega_R(\sigma = 0)}. \quad (\text{C11})$$

Finally, because the detuning is zero, the spectrum is completely symmetrical. The effective Rabi splitting is simply twice the absolute value of the lower polariton energy, which yields Eq. (28).

APPENDIX D: DERIVATION OF EFFECTIVE RABI SPLITTING UNDER STATIC AND DYNAMIC ANGULAR DISORDER

In this Appendix we use a cumulant expansion to calculate the effective Rabi splitting that is relevant with disorder as a function of the disorder strength σ and/or correlation time τ_c . At this point, if we ignore the pumping and non-Hermitian decay from Eqs. (9)–(13), the Hamiltonian of the disordered system is

$$\hat{H} = H_0 + \Lambda_\theta, \quad (\text{D1})$$

$$H_0 = E_v |v\rangle\langle v| + \sum_{m=1}^N E_m |m\rangle\langle m|, \quad (\text{D2})$$

$$\Lambda_\theta = \sum_{m=1}^N V_{mv}(\theta_m) |m\rangle\langle v| + V_{vm}(\theta_m) |v\rangle\langle m|. \quad (\text{D3})$$

As shown in Eq. (19), dynamic angular disorder enters as a modulation of θ in the coupling $V_{mv}(\theta_m) = V \cos(\theta_m)$ between each individual emitter and the bare cavity mode. It is straightforward to obtain the instantaneous eigenvalues of H because the characteristic polynomial is

$$\lambda^{N-1} \left(\lambda^2 - \sum_{m=1}^N V^2 \cos^2(\theta_m) \right) = 0. \quad (\text{D4})$$

Hence, the effective Rabi splitting is $\Omega_R/\Omega_R(\sigma = 0) = \sqrt{\langle \cos^2 \theta_m \rangle}$, where $\theta_m(t)$ satisfies $\langle \theta_m(t) \rangle = 0$ and $\langle \theta_m(t_j) \theta_n(t_k) \rangle = \delta_{mn} \sigma^2 \exp(-|t_j - t_k|/\tau_c)$. By cumulant

TABLE I. Symbols; energies, rates, or frequencies; and values that appear in this paper.

Symbol	Energy, rate, or frequency	Value
E_v	cavity mode energy	0
E_m	molecular singly excited-state energy	0
\hat{V}_{mv}	coupling between cavity mode $ v\rangle$ and molecular excited state $ m\rangle$	$0.5/\sqrt{N}$
\hat{V}_{m0}	coupling between ground state $ 0\rangle$ and molecular excited state $ m\rangle$	0.0005
$E_0 + \hbar\omega$	single-photon dressed molecular ground state	$[-1.2, 1.2]$
Γ_{rad}	single molecule radiative decay rate	$0.05/N$
Γ_{loc}	local relaxation rate	0.05
$\Gamma_{\text{cav}}(\Gamma_{\text{cav}}^R + \Gamma_{\text{cav}}^{NR})$	cavity leakage rate (including radiative and nonradiative)	0.05
σ	standard deviation	$0 \rightarrow 0.3$ (energy), $0 \rightarrow 0.6\pi$ (angle)
τ_c	correlation time	$0.1 \rightarrow 100$ (dynamic \rightarrow static)

expansion

$$\langle |\cos \theta_m| \rangle = \text{Re} \left[\exp \left(i \langle \theta_m \rangle - \frac{1}{2} \langle \delta \theta_m^2 \rangle \right) \right] = \exp(-\sigma^2/2). \quad (\text{D5})$$

Hence, in the static limit ($\tau_c = \infty$),

$$\langle \cos^2 \theta_m \rangle = \left\langle \frac{\cos 2\theta_m + 1}{2} \right\rangle = \frac{e^{-2\sigma^2} + 1}{2}. \quad (\text{D6})$$

The effective Rabi splitting is

$$\Omega_R(\sigma, \tau_c = \infty) / \Omega_R(\sigma = 0) = \sqrt{(e^{-2\sigma^2} + 1)/2}. \quad (\text{D7})$$

This analytical formula is verified in Fig. 15. The numerical results are extracted from Fig. 7.

In the fast modulation limit ($\tau_c = 0$), the external field sees an averaged upper or lower polariton state [as defined in Eq. (C5)], which leads to average Rabi splitting

$$\Omega_R(\sigma, \tau_c = 0) / \Omega_R(\sigma = 0) = \langle |\cos \theta_m| \rangle = e^{-\sigma^2/2}. \quad (\text{D8})$$

Unfortunately, we have not yet been able to derive an analytic form for the effective Rabi splitting for finite τ_c . For a general τ_c , the effective Rabi splitting is not determined exclusively by the instantaneous eigenvalues [which allowed us to calculate the slow and fast limits (D7) and (D8) above]. Nevertheless, in Fig. 15 we plot the effective Rabi splitting for two different values of N (the number of emitters). Note that the two lines are on top of one another. Thus, even though we do not have a predictive theory for the Rabi splitting in the intermediate τ_c regime, we can at least be confident that the Rabi splitting

always scales as \sqrt{N} (which would seem to agree with the results in Ref. [69]).

APPENDIX E: ENERGIES, RATES, AND FREQUENCIES

In this Appendix we list all the parameters in the paper. For the model with a cavity, we choose to normalize the Rabi splitting for the no-disorder system and thus all parameters listed in Table I are in units of $\Omega_R(\sigma = 0)$. In the strong-coupling regime, the Rabi splitting should be greater than the linewidth of the observed polariton peaks [$\Omega_R(\sigma = 0) > \Gamma$], which is determined by both lifetime and all types of disorders. Conveniently, we choose the total decay rate to be $\Gamma_{\text{tot}} = \Gamma_{\text{cav}} + \Gamma_{\text{loc}} = 0.1\Omega_R(\sigma = 0)$, namely, the natural linewidth is a tenth of the Rabi splitting for cases with no disorder. The choices of standard deviation and correlation time aim to show the qualitative behaviors of line shape under different types of disorder. Specifically, the correlation time ranges from static ($\tau_c \rightarrow \infty$, corresponding to the low-temperature regime) to dynamic ($\tau_c \rightarrow 0$, corresponding to very strong pure dephasing in the high-temperature regime).

For the model without a cavity, we choose to keep all identical parameters the same. For example, in order to keep the no-disorder linewidth the same, the collective radiative decay rate is chosen to be $\Gamma_{\text{rad}} = \Gamma_{\text{cav}}/N$. This choice should be valid because, in reality, the linewidth of absorption outside a cavity and the linewidth of reflection or transmission inside a cavity are of the same order of magnitude.

Finally, the remaining parameters (\hat{V}_{m0} , $E_0 + \hbar\omega$, and $E_v = E_m$) are only used for calculating steady-state results. The results do not depend on choices of $E_0 + \hbar\omega$. The \hat{V}_{m0} is an arbitrary small number and determines only the magnitude of the flux but not the line shape.

[1] R. H. Dicke, Coherence in spontaneous radiation processes, *Phys. Rev.* **93**, 99 (1954).

[2] M. Tavis and F. W. Cummings, Exact solution for an N -molecule–radiation–field Hamiltonian, *Phys. Rev.* **170**, 379 (1968).

[3] F. C. Spano and S. Mukamel, Superradiance in molecular aggregates, *J. Chem. Phys.* **91**, 683 (1989).

[4] S.-H. Lim, T. G. Bjorklund, F. C. Spano, and C. J. Bardeen, Exciton Delocalization and Superradiance in Tetracene Thin Films and Nanoaggregates, *Phys. Rev. Lett.* **92**, 107402 (2004).

- [5] J. Larson and T. Mavrogordatos, *The Jaynes-Cummings Model and Its Descendants: Modern Research Directions* (IOP, Bristol, 2021).
- [6] R. Bonifacio and L. Lugiato, Cooperative radiation processes in two-level systems: Superfluorescence, *Phys. Rev. A* **11**, 1507 (1975).
- [7] G. Rainò, M. A. Becker, M. I. Bodnarchuk, R. F. Mahrt, M. V. Kovalenko, and T. Stöferle, Superfluorescence from lead halide perovskite quantum dot superlattices, *Nature (London)* **563**, 671 (2018).
- [8] J. M. Raimond, P. Goy, M. Gross, C. Fabre, and S. Haroche, Collective Absorption of Blackbody Radiation by Rydberg Atoms in a Cavity: An Experiment on Bose Statistics and Brownian Motion, *Phys. Rev. Lett.* **49**, 117 (1982).
- [9] C. Weisbuch, M. Nishioka, A. Ishikawa, and Y. Arakawa, Observation of the Coupled Exciton-Photon Mode Splitting in a Semiconductor Quantum Microcavity, *Phys. Rev. Lett.* **69**, 3314 (1992).
- [10] D. J. Heinzen, J. J. Childs, J. E. Thomas, and M. S. Feld, Enhanced and Inhibited Visible Spontaneous Emission by Atoms in a Confocal Resonator, *Phys. Rev. Lett.* **58**, 1320 (1987).
- [11] W. Jhe, A. Anderson, E. A. Hinds, D. Meschede, L. Moi, and S. Haroche, Suppression of Spontaneous Decay at Optical Frequencies: Test of Vacuum-Field Anisotropy in Confined Space, *Phys. Rev. Lett.* **58**, 666 (1987).
- [12] F. De Martini, G. Innocenti, G. R. Jacobovitz, and P. Mataloni, Anomalous Spontaneous Emission Time in a Microscopic Optical Cavity, *Phys. Rev. Lett.* **59**, 2955 (1987).
- [13] M. Bayer, T. L. Reinecke, F. Weidner, A. Larionov, A. McDonald, and A. Forchel, Inhibition and Enhancement of the Spontaneous Emission of Quantum Dots in Structured Microresonators, *Phys. Rev. Lett.* **86**, 3168 (2001).
- [14] R. Houdré, R. P. Stanley, U. Oesterle, M. Ilegems, and C. Weisbuch, Room-temperature cavity polaritons in a semiconductor microcavity, *Phys. Rev. B* **49**, 16761 (1994).
- [15] J.-M. Gérard, B. Sermage, B. Gayral, B. Legrand, E. Costard, and V. Thierry-Mieg, Enhanced Spontaneous Emission by Quantum Boxes in a Monolithic Optical Microcavity, *Phys. Rev. Lett.* **81**, 1110 (1998).
- [16] T. Yoshie, A. Scherer, J. Hendrickson, G. Khitrova, H. Gibbs, G. Rupper, C. Ell, O. Shchekin, and D. Deppe, Vacuum Rabi splitting with a single quantum dot in a photonic crystal nanocavity, *Nature (London)* **432**, 200 (2004).
- [17] D. J. Masiello and G. C. Schatz, Many-body theory of surface-enhanced Raman scattering, *Phys. Rev. A* **78**, 042505 (2008).
- [18] F. C. Spano, The Spectral Signatures of Frenkel Polarons in H- and J-Aggregates, *Acc. Chem. Res.* **43**, 429 (2010).
- [19] N. Mirsaleh-Kohan, V. Ileri, P. D. Simmons, Jr., N. W. Bigelow, A. Vaschillo, M. M. Rowland, M. D. Best, S. J. Pennycook, D. J. Masiello, B. S. Gupton, and J. P. Camden, Single-molecule surface-enhanced Raman scattering: Can STEM/EELS image electromagnetic hot spots? *J. Phys. Chem. Lett.* **3**, 2303 (2012).
- [20] F. C. Spano, Optical microcavities enhance the exciton coherence length and eliminate vibronic coupling in J-aggregates, *J. Chem. Phys.* **142**, 184707 (2015).
- [21] F. Herrera and F. C. Spano, Cavity-Controlled Chemistry in Molecular Ensembles, *Phys. Rev. Lett.* **116**, 238301 (2016).
- [22] F. Herrera and F. C. Spano, Absorption and photoluminescence in organic cavity QED, *Phys. Rev. A* **95**, 053867 (2017).
- [23] I. Abid, W. Chen, J. Yuan, A. Bohloul, S. Najmaei, C. Avendano, R. Péchou, A. Mlayah, and J. Lou, Temperature-dependent plasmon-exciton interactions in hybrid Au/MoSe₂ nanostructures, *ACS Photon.* **4**, 1653 (2017).
- [24] A. Bisht, J. Cuadra, M. Wersall, A. Canales, T. J. Antosiewicz, and T. Shegai, Collective strong light-matter coupling in hierarchical microcavity-plasmon-exciton systems, *Nano Lett.* **19**, 189 (2019).
- [25] M. Hertzog, M. Wang, J. Mony, and K. Börjesson, Strong light-matter interactions: A new direction within chemistry, *Chem. Soc. Rev.* **48**, 937 (2019).
- [26] D. Sidler, C. Schäfer, M. Ruggenthaler, and A. Rubio, Polaritonic chemistry: Collective strong coupling implies strong local modification of chemical properties, *J. Phys. Chem. Lett.* **12**, 508 (2021).
- [27] K. C. Smith, A. Bhattacharya, and D. J. Masiello, Exact k -body representation of the Jaynes-Cummings interaction in the dressed basis: Insight into many-body phenomena with light, *Phys. Rev. A* **104**, 013707 (2021).
- [28] T. E. Li, B. Cui, J. E. Subotnik, and A. Nitzan, Molecular polaritonics: Chemical dynamics under strong light-matter coupling, *Annu. Rev. Phys. Chem.* **73**, 43 (2022).
- [29] B. Renaud, R. Whitley, and C. Stroud, Jr., Nonstationary two-level resonance fluorescence, *J. Phys. B* **10**, 19 (1977).
- [30] M. Gross and S. Haroche, Superradiance: An essay on the theory of collective spontaneous emission, *Phys. Rep.* **93**, 301 (1982).
- [31] G. Celardo, A. Biella, L. Kaplan, and F. Borgonovi, Interplay of superradiance and disorder in the Anderson model, *Fortschr. Phys.* **61**, 250 (2013).
- [32] A. Biella, F. Borgonovi, R. Kaiser, and G. Celardo, Subradiant hybrid states in the open 3D Anderson-Dicke model, *Europhys. Lett.* **103**, 57009 (2013).
- [33] A. Delga, J. Feist, J. Bravo-Abad, and F. J. Garcia-Vidal, Quantum Emitters Near a Metal Nanoparticle: Strong Coupling and Quenching, *Phys. Rev. Lett.* **112**, 253601 (2014).
- [34] G. L. Celardo, G. G. Giusteri, and F. Borgonovi, Cooperative robustness to static disorder: Superradiance and localization in a nanoscale ring to model light-harvesting systems found in nature, *Phys. Rev. B* **90**, 075113 (2014).
- [35] V. N. Pustovit, A. M. Urbas, and T. V. Shahbazyan, Energy transfer in plasmonic systems, *J. Opt.* **16**, 114015 (2014).
- [36] A. Goban, C.-L. Hung, J. D. Hood, S.-P. Yu, J. A. Muniz, O. Painter, and H. J. Kimble, Superradiance for Atoms Trapped along a Photonic Crystal Waveguide, *Phys. Rev. Lett.* **115**, 063601 (2015).
- [37] M. A. Norcia, M. N. Winchester, J. R. Cline, and J. K. Thompson, Superradiance on the millihertz linewidth strontium clock transition, *Sci. Adv.* **2**, e1601231 (2016).
- [38] A. Asenjo-Garcia, M. Moreno-Cardoner, A. Albrecht, H. J. Kimble, and D. E. Chang, Exponential Improvement in Photon Storage Fidelities Using Subradiance and “Selective Radiance” in Atomic Arrays, *Phys. Rev. X* **7**, 031024 (2017).
- [39] P. Kirton and J. Keeling, Suppressing and Restoring the Dicke Superradiance Transition by Dephasing and Decay, *Phys. Rev. Lett.* **118**, 123602 (2017).
- [40] T. V. Shahbazyan, M. E. Raikh, and Z. V. Vardeny, Mesoscopic cooperative emission from a disordered system, *Phys. Rev. B* **61**, 13266 (2000).

- [41] M. Sukharev and A. Nitzan, Optics of exciton-plasmon nano-materials, *J. Phys.: Condens. Matter* **29**, 443003 (2017).
- [42] P. Fauché, C. Gebhardt, M. Sukharev, and R. A. Vallée, Plasmonic opals: Observation of a collective molecular exciton mode beyond the strong coupling, *Sci. Rep.* **7**, 4107 (2017).
- [43] R. F. Ribeiro, L. A. Martínez-Martínez, M. Du, J. Campos-Gonzalez-Angulo, and J. Yuen-Zhou, Polariton chemistry: Controlling molecular dynamics with optical cavities, *Chem. Sci.* **9**, 6325 (2018).
- [44] F. Herrera and F. C. Spano, Theory of nanoscale organic cavities: The essential role of vibration-photon dressed states, *ACS Photon.* **5**, 65 (2018).
- [45] M. Gómez-Castaño, A. Redondo-Cubero, L. Buisson, J. L. Pau, A. Mihi, S. Ravaine, R. A. Vallée, A. Nitzan, and M. Sukharev, Energy transfer and interference by collective electromagnetic coupling, *Nano Lett.* **19**, 5790 (2019).
- [46] S. Wang, G. D. Scholes, and L.-Y. Hsu, Quantum dynamics of a molecular emitter strongly coupled with surface plasmon polaritons: A macroscopic quantum electrodynamics approach, *J. Chem. Phys.* **151**, 014105 (2019).
- [47] S. Wang, G. D. Scholes, and L.-Y. Hsu, Coherent-to-incoherent transition of molecular fluorescence controlled by surface plasmon polaritons, *J. Phys. Chem. Lett.* **11**, 5948 (2020).
- [48] F. Mattiotti, M. Kuno, F. Borroni, B. Jankó, and G. L. Celardo, Thermal decoherence of superradiance in lead halide perovskite nanocrystal superlattices, *Nano Lett.* **20**, 7382 (2020).
- [49] S. Wang, M.-W. Lee, Y.-T. Chuang, G. D. Scholes, and L.-Y. Hsu, Theory of molecular emission power spectra. I. Macroscopic quantum electrodynamics formalism, *J. Chem. Phys.* **153**, 184102 (2020).
- [50] F. C. Spano, Exciton-phonon polaritons in organic microcavities: Testing a simple ansatz for treating a large number of chromophores, *J. Chem. Phys.* **152**, 204113 (2020).
- [51] S. Wang, L.-Y. Hsu, Exploring superradiance effects of molecular emitters coupled with cavity photons and plasmon polaritons: A perspective from macroscopic quantum electrodynamics., *J. Phys. Chem. C* (2023).
- [52] M.-W. Lee, Y.-T. Chuang, and L.-Y. Hsu, Theory of molecular emission power spectra. II. Angle, frequency, and distance dependence of electromagnetic environment factor of a molecular emitter in plasmonic environments, *J. Chem. Phys.* **155**, 074101 (2021).
- [53] S. Wang, Y.-T. Chuang, and L.-Y. Hsu, Simple but accurate estimation of light-matter coupling strength and optical loss for a molecular emitter coupled with photonic modes, *J. Chem. Phys.* **155**, 134117 (2021).
- [54] F. Herrera and M. Litinskaya, Disordered ensembles of strongly coupled single-molecule plasmonic picocavities as nonlinear optical metamaterials, *J. Chem. Phys.* **156**, 114702 (2022).
- [55] H.-T. Chen, Z. Zhou, M. Sukharev, J. E. Subotnik, and A. Nitzan, Interplay between disorder and collective coherent response: Superradiance and spectral motional narrowing in the time domain, *Phys. Rev. A* **106**, 053703 (2022).
- [56] N. Skribanowitz, I. Herman, J. MacGillivray, and M. Feld, Observation of Dicke Superradiance in Optically Pumped HF Gas, *Phys. Rev. Lett.* **30**, 309 (1973).
- [57] S. Prasad and R. J. Glauber, Polarium model: Coherent radiation by a resonant medium, *Phys. Rev. A* **61**, 063814 (2000).
- [58] M. O. Scully and A. A. Svidzinsky, The super of superradiance, *Science* **325**, 1510 (2009).
- [59] Limiting the model to a single cavity mode that is closest to the molecular excitation frequency assumes that line broadening is small relative to intermode spacing, which holds far outside the ultrastrong-coupling regime.
- [60] A. V. Kavokin, J. J. Baumberg, G. Malpuech, and F. P. Laussy, *Microcavities*, Vol. 21 (Oxford University Press, Oxford, 2017).
- [61] U. Akram, Z. Ficek, and S. Swain, Decoherence and coherent population transfer between two coupled systems, *Phys. Rev. A* **62**, 013413 (2000).
- [62] The choice of intermolecular coupling is 0.1 in units of Rabi splitting. Rabi splitting is approximately on the order of 10 meV, and if the distance between dipoles is 2 nm, the dipole moments are on the order of 10 D.
- [63] R. Kubo and K. Tomita, A general theory of magnetic resonance absorption, *J. Phys. Soc. Jpn.* **9**, 888 (1954).
- [64] R. Kubo, The fluctuation-dissipation theorem, *Rep. Prog. Phys.* **29**, 255 (1966).
- [65] A. Nitzan, *Chemical Dynamics in Condensed Phases: Relaxation, Transfer and Reactions in Condensed Molecular Systems* (Oxford University Press, Oxford, 2006), Chap. 7.
- [66] R. Houdré, R. P. Stanley, and M. Heger, Vacuum-field Rabi splitting in the presence of inhomogeneous broadening: Resolution of a homogeneous linewidth in an inhomogeneously broadened system, *Phys. Rev. A* **53**, 2711 (1996).
- [67] B. Cui and A. Nitzan, Collective response in light-matter interactions: The interplay between strong coupling and local dynamics, *J. Chem. Phys.* **157**, 114108 (2022).
- [68] G. B. Rybicki, Notes on Gaussian random functions with exponential correlation functions (Ornstein-Uhlenbeck process), available at https://www.lanl.gov/DLDSTP/fast/OU_process.pdf (unpublished).
- [69] J. B. Pérez-Sánchez *et al.*, Simulating molecular polaritons in the collective regime using few-molecule models, *Proc. Natl. Acad. Sci.* **120**, e2219223120 (2023).